Vol.1, pp.14-19, 2014

International Journal of Scientific Research & Engineering Technology (IJSET)
Noura et al./IPCO-2014

ASPECT RATIO EFFECTS ON 3D INCOMPRESSIBLE FLOW IN LID DRIVEN PARALLEPIPED CAVITY

Noura BEN MANSOUR*, Nader BEN-CHEIKH* and Brahim BEN-BEYA*

** Laboratory of Fluid Dynamics, Physics Department, Faculty of Sciences of Tunis, Campus Universitaire, 2092 El-Manar II, Tunisia.*

benmansournoura@yahoo.fr

Abstract— **A numerical study of the three-dimensional fluid flow has been carried out to determine the effects of the transverse aspect ratio, Ay, on the flow structure in lid-driven cavities. The numerical method is based on the finite volume method and multigrid acceleration. Computations have been investigated for several Reynolds numbers, Richardson numbers and various aspect ratio values. At a fixed Reynolds number, Re = 100, the three-dimensional flow characteristics are analyzed considering three transverse aspect ratios, Ay = 1, 0.5 and 0.25. The results are presented in terms of distributions of streamlines, isotherms and average Nusselt number. We note tha t the heat transfer rate increasing by increasing the aspect ratio and the Richardson number.**

Keywords— **Fluid mechanics; 3D driven cavity; Finite volumes method; Multigrid; Aspect ratio.**

I. INTRODUCTION

In recent years the mixed convection in rectangular or square cavities has been investigated by many researchers. This attempt is due to the fact that heat transfer in a square cavity can be found in many industrial and engineering applications such as electronic component cooling, food drying process, nuclear reactors etc… Flow and heat transfer phenomena caused by buoyancy and shear forces in enclosures have been studied extensively in the literature. For example, Iwatsu [1] numerically studied three dimensional flows in cubical containers. The top moving wall is maintained at a higher temperature than the bottom wall. Numerical solutions are obtained over a wide range of physical parameters, $102 \leq Re \leq 2\times103$, $0 \leq Ri \leq 10$ and $Pr = 0.71$. Numerical flow visualizations demonstrate the explicit effects of Ri as well as Re. Mohamed and Viskanta [2] investigated the effects of a sliding lid on the fluid flow and thermal structures in a shallow lid-driven cavity. Moallemi and Jang [3] studied numerically mixed convective flows in a bottom heated square lid-driven enclosure. They investigated the effect of Prandtl number on the flow and heat transfer process. They found that the effects of buoyancy are more pronounced for higher values of Prandtl numbers, and they also derived a correlation for the average Nusselt number in terms of the Prandtl number, Reynolds number and Richardson number. Prasad and Koseff [4] performed an experimental investigation of mixed convection flow in a lid-driven cavity for a different Richardson numbers, ranging from 0.1 to 1000. Their results indicate that the overall heat transfer rate is a very weak function of the Grashof number for the examined range of Reynolds numbers. They have also analyzed the mean heat flux values over the entire boundary to produce Nusselt number and Stanton number correlations which are very useful for design applications. Sharif [5] performed a numerical investigation with supplementary flow visualization of laminar mixed convective heat transfer in two-dimensional shallow rectangular driven cavities of aspect ratio 10. The top moving plate of the cavity is set at a higher temperature than the bottom stationary plate. Computations are reported for Rayleigh numbers ranging from 105 to 107 while keeping the Reynolds number fixed at 408.21, thus encompassing the wide spectrum of dominating forced convection, mixed convection, and dominating natural convection flow regimes. A numerical study of the three-dimensional fluid flow has been carried out to determine the effects of the transverse aspect ratio, Ay, on the flow structure in lid-driven cavities was investigated by Nader [6] and Fakher [7].

The objective of this work is to study the effect of aspect ratio, varied from 0.25 to the unity, on the overall structure of the flow. Thus, the Richardson number ranging from 0.001 to 10 were considered.

II. MATHEMATICAL FORMULATION

II.1. GOVERNING EQUATIONS

For laminar, incompressible and three-dimensional mixed convection, after invoking the Boussinesq approximation and neglecting the viscous dissipation, can be expressed in the dimensionless form as:
Continuity equation:

$$\frac{\partial u_i}{\partial x_i} = 0 \quad (1)$$

Three momentum equations:

$$\frac{\partial u_i}{\partial t} + \frac{\partial (u_i u_i)}{\partial x_j} = -\frac{\partial P}{\partial x_i} + \frac{1}{\mathrm{Re}}\left(\frac{\partial^2 u_i u_i}{\partial x_i \partial x_i}\right) + Ri\theta\delta_{i3} \quad (2)$$

Energy equation:

$$\frac{\partial \theta}{\partial t} + \frac{\partial (u_i \theta)}{\partial x_i} = \frac{1}{\mathrm{Re}\,\mathrm{Pr}}\left(\frac{\partial^2 \theta}{\partial x_i \partial x_i}\right) \quad (3)$$

Where, u , v and w are the velocity components in the x, y and z directions, respectively, θ is the temperature and P is the pressure. ρ is the mass density and g is the gravitational acceleration. In Eq. (2), the symbol δ stands for the Krönecker delta. The chosen scales in Eqs. (1)– (3) are the length H , the velocity $u_0 = \sqrt{g\beta H \Delta T}$, the time $t_0 = \frac{H}{u_0}$ and the pressure $P_0 = \rho u_0^2$. Further, the non-dimensional temperature is defined by $\theta = (T - T_r)(T_{hot} - T_{cold})$, where the reference temperature is $T_r = \frac{(T_{hot} + T_{cold})}{2}$. The non-dimensional numbers seen above, Gr, Re, Pr and Ri are the Grashof number, Reynolds number, Prandtl number and Richardson number, respectively, and they are defined as:

$Gr = \frac{g\beta\Delta T L^3}{\nu^2}$, $\mathrm{Re} = \frac{u_0 L}{\nu}$, $\mathrm{Pr} = \frac{\nu}{\alpha}$ and $Ri = \frac{Gr}{\mathrm{Re}^2}$.

II.2 Initial and Boundary conditions

No slip condition at bottom and side walls. The upper lid has a constant velocity, u_0. The horizontal upper lid wall has an isothermal condition with temperature, $T=T_H$. The bottom wall is at rest and isotherm, i.e., $T=T_C$ ($T_C < T_H$). Finally, the remaining walls are adiabatic (see Fig.1).

II.3. Numerical procedure

In the FORTRAN code, the unsteady Navier–Stokes and energy equations are discretized by a second-order time stepping finite difference procedure. The procedure adopted here deserves a detailed explanation. First, the non-linear terms in Eqs. (2) are treated explicitly with a second-order Adams–Bashforth scheme. Second, the convective terms in Eq. (3) are treated semi implicitly. Third, the diffusion terms in Eqs. (2) and (3) are treated implicitly. In order to avoid the difficulty that the strong velocity-pressure coupling brings forward, we selected a projection method described in Peyret and Taylor [9] and Achdou and Guermond [10].

A finite-volume method is implemented to discretize the Navier–Stokes and energy equations (Patankar [11], F. Moukhalled and M. Darwish [12], Kobayachi and Pereira [13]).

The advective terms in Eqs. (2) are discretized using a QUICK third-order scheme whereas a second-order central differencing (Hayase, Humphrey and Greif [14]) is applied in Eq. (3). The discretized momentum and energy equations are solved employing the red and black successive over relaxation method (RBSOR) [15], while the Poisson pressure correction equation is solved utilizing a full multi-grid method (Hortmann, Peric and Scheuerer [16], M.S. Mesquita and M.J.S. de Lemos [17], E. Nobile [18]). If specific details about the computational methodology are needed, the reader is directed to Ben-Cheikh et al. [19]. Finally, the convergence of solutions is assumed when the relative error for each variable between consecutive iterations is recorded below the convergence criterion ε such that:

$$\sum_{i,j,k} \left| \phi_{ijk}^{m+1} - \phi_{ijk}^{m} \right| \le \varepsilon$$

Here, ϕ represents a dependent variable u, v, w, or θ, the indexes i, j, k indicate a grid point, and the index m is the current iteration at the grid level. The convergence criterion was set to 10^{-6}.

III. Results and Discussion

III.1. Test case

Simulations were performed by using our three-dimensional finite volume code for the test case of a 3D lid-driven cubic cavity and validated with respect to Wong et al. [1] works. We have chosen to use a grid of 483 nodes refined near the walls. In fact, the selected mesh size provides a good compromise between accuracy and CPU time in the range of Reynolds numbers to be investigated. Fig. 1 shows a comparison of u - and w-velocity profiles along the centerline of the lid-driven cubical cavity of the present work with Ref. [1] at the Reynolds numbers (Re = 100 and 1000). Our data as well as the centerline profiles seem to be in good agreement with the results of Ref. [1].

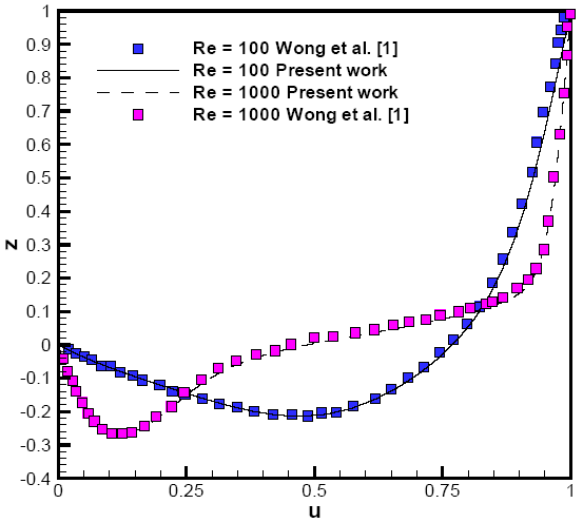

Fig.2. Comparison of u -and w -velocity components distribution along the centreline of cubic cavity of the present work with Ref. [1] for Re = 100 and 1000.

III.2. Aspect ratio effects

In what follows, we will present a detailed analysis of the aspect ratio effects on the three dimensional flows in lid-driven cavity for the steady solution obtained at Re =100 and 1000. For this Reynolds number, the Richardson number is varied from 0.001 to 10, three transverse aspect ratios Ay = 1, 0.5 and 0.25 are considered. It is worth noting that Ax is maintained to 1 in all simulations. In Fig. 3 are presented the u contours at the mid-plane (y = 0.5) of the cavity for Ay = 1, 0.5 and 0.25. Two rolls are observed for both components: two symmetrical clockwise and anticlockwise rolls close to the walls. The intensity of the two rolls seems to become feeble by lowering the aspect ratio from the unit to 0.25 and by increasing the Richardson number for the two Reynolds number. The same trend is observed in the two Reynolds numbers.

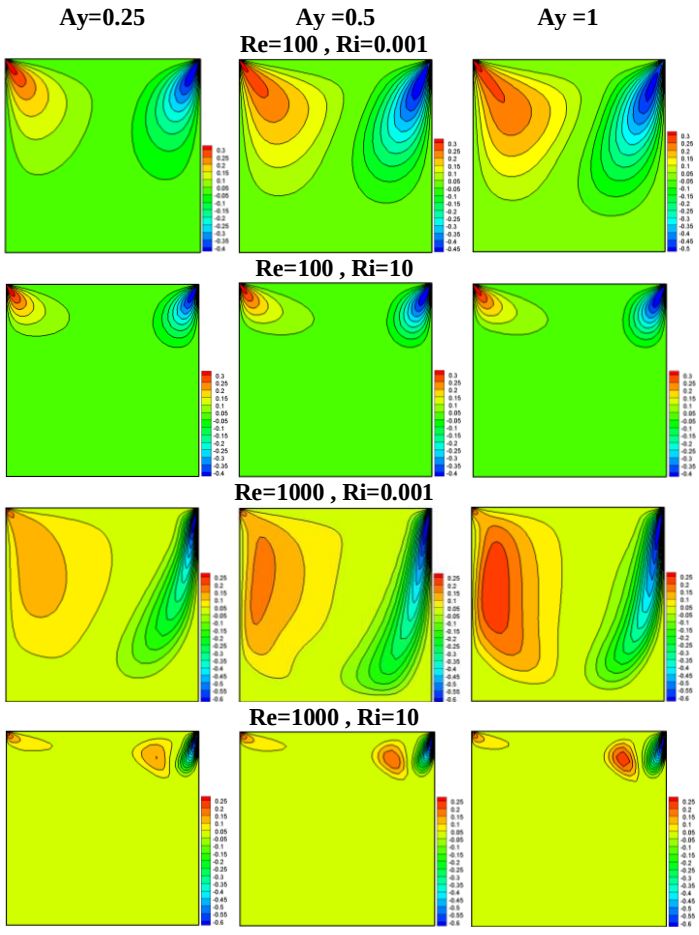

Fig.3: Contours of u -and w -velocity components at the mid-plane (y = 0.5) for Re = 100 and 1000, Ay = 1, 0.5 and 0.25.

In Fig. 4 and Fig. 5 are presented the mid-plane streamlines distributions for designated values of Re, Ri and aspect ratio. When Re=100, Ri = 10 and Ay= 1, the flow patterns are characterized by three primary recirculating counter-rotating vortices. This behavior is primarily due to the lid movement that occupies the region near the hot sliding wall.

In addition, a minor secondary recirculating vortex due to buoyancy is observed near the bottom wall. With decrements in Ay from the unity to 0.25, the bottom cell becomes feeble and amalgamates with the upper adjacent cell to provide only two extensive clockwise and anticlockwise vortices close to the walls. When Re=100, Ri = 0.001 and for different aspet ratio, a single primary vortex is observed covering most of the cavity domain. The intensity of the vortex seems to become feeble by lowering the aspect ratio from the unit to 0.25.

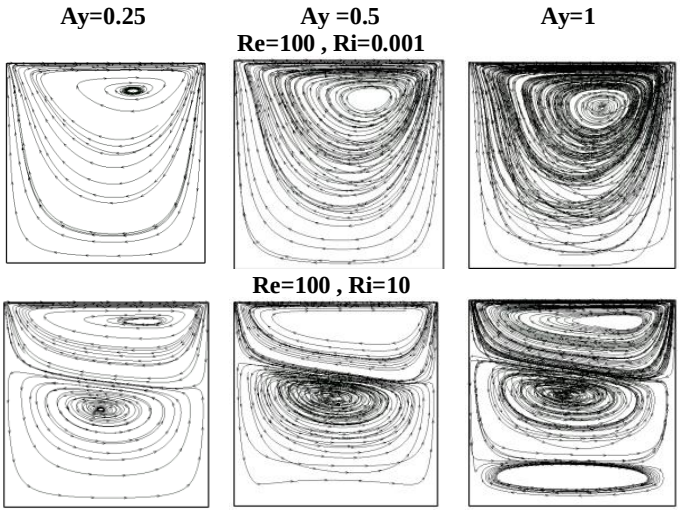

Fig. 4: Stream traces at the mid-plane (y = 0.5) at Re = 100 for the three aspect ratio values Ay = 1, 0.5 and 0.25 for Ri = 10 and 0.001.

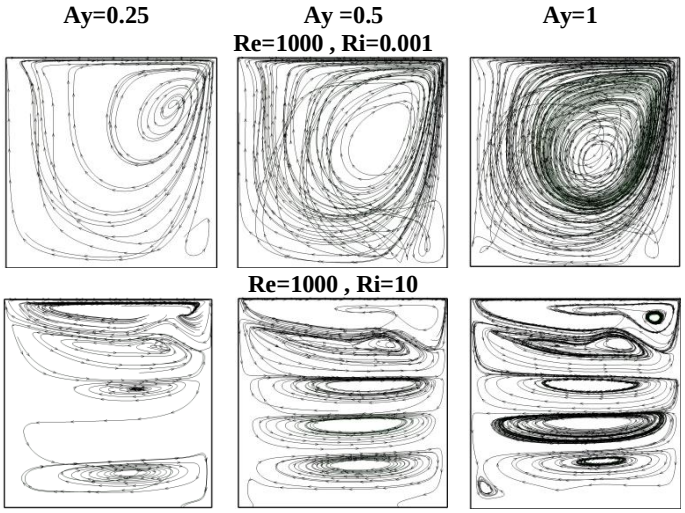

Fig. 5: Stream traces at the mid-plane (y = 0.5) at Re = 1000 for the three aspect ratio values Ay =1, 0.5 and 0.25 for Ri = 10 and 0.001.

When Re=1000, Ri = 10 and Ay= 1, the flow are characterized by six counter-rotating vortices. With the decrease of aspect ratio to 0.25, we note the decrease of the number of the vortices. When Ri = 0.001, the flow structure is characterized by the presence of one cell covering the whole

area of the cavity, the center of the cell moves the middle of the cavity to the upper right corner.

Fig. 6 and Fig. 7 illustrate the influence of varying Re, Ri and aspect ratio on the isotherms for the cases studied. The results convincingly indicate that when Ri is set at 10, the isotherms exhibit similar trends for different aspect ratio. Consequently, the collective behavior attests the impact that Re exerts on heat transfer is insignificant. Accordingly, since the buoyancy is high (Ri=10), the temperature contours embody a thermally stratified situation.

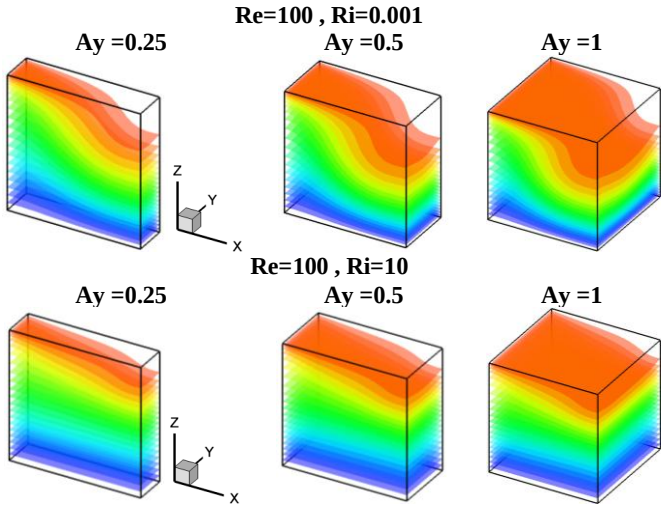

Fig. 6: The isotherm plots for Re = 100, Ri =0.001 and 10 and for the different aspect ratio

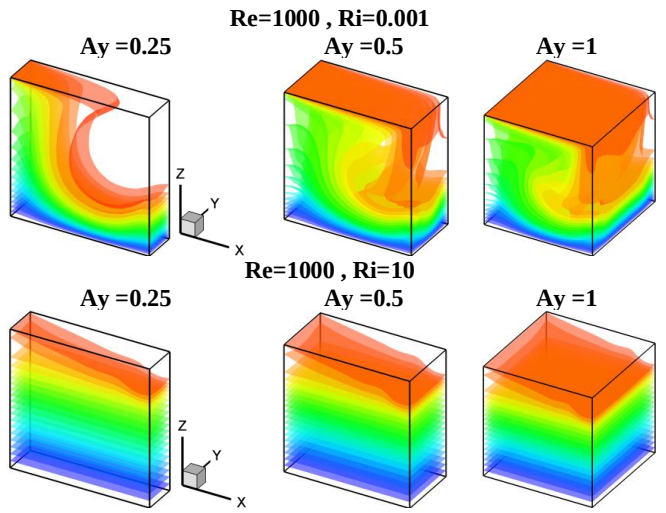

Fig. 7: The isotherm plots for Re = 1000 Ri =0.001 and10 and for the different aspect ratio

In other words, the flow is principally dominated by buoyancy and the heat transfer is controlled mainly by conduction, implying that forced convection due to the lid-movement is almost absent. The results convincingly indicate that when aspect ratio increases to Ay=1 and Ri is feeble i.e., Ri = 0.001, the results indicate the buoyancy effects remain dominant.

When Re = 1000 and Ri = 10, there is a thermal stratification for all Richardson numbers. The heat transfer is controlled mainly by conduction, implying that forced convection due to the lid movement is almost absent. In other hand, we note that the temperature distribution is very sensitive to the change of aspect ratio.

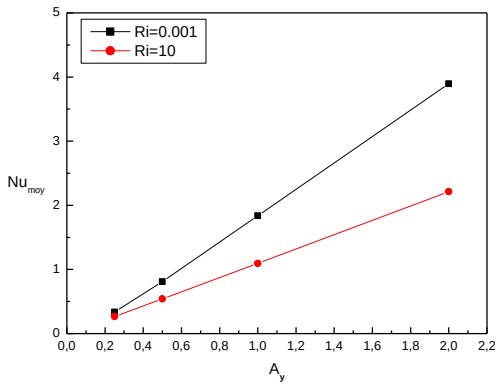

Fig.8. Variation in the average Nusselt number with aspect ratio at different Richardson numbers for Re 100.

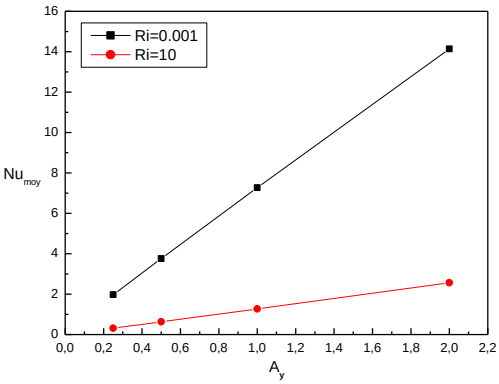

Fig.9. Variation in the average Nusselt number with aspect ratio at different Richardson numbers for Re 1000.

Fig.8.and Fig.9 show the average Nusselt number variation with the aspect ratio at different Richardson numbers for Re 100 and 1000, respectively. The results indicate that the average Nusselt number increases by increasing of the Reynolds number. On the other hand, due to the increase in the body force effects with increasing Richardson number, a clear increase in the Nusselt number with the aspect ratio is noticed.

Fig.10 and Fig.11 show u and w velocity components distribution along the centerline of cubic cavity for Re = 100 and for different Richardson number. The subfigure 10-a shows that in the lower part of the cavity, the u-velocity component is negative while it's positive in the rest of the cavity which proves the presence of a clockwise rotating cell which occupies the entire cavity. A minimum value of the u-

velocity component (-0.214) is observed for a aspect ratio Ay = 1.

The subfigure 10-b shows that the u-velocity component is zero at the lower half of the cavity. This component is negative in the lower part of the upper half of the cavity and positive in the rest, indicating the presence of a rotating cell clockwise at the upper half of the cavity. The same behavior is observed for the three aspect ratios studied.

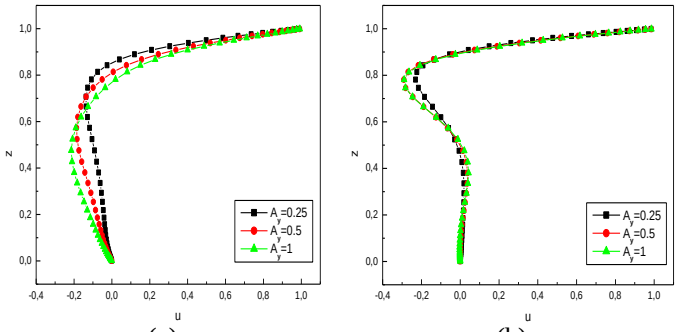

(a) (b)

Fig.10.u-velocity components distribution along the centerline of cubic cavity for Re = 100 at (a) Ri = 0.001 and (b) Ri = 10

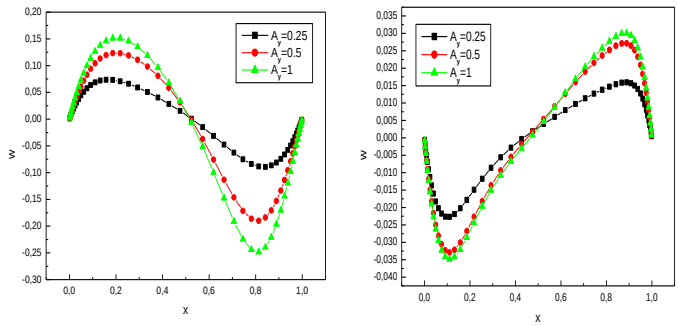

(a) (b)

Fig.11.w-velocitycomponents distribution along the centerline of cubic cavity for Re = 100 at (a) Ri = 0.001and (b) Ri = 10

The figure 10 shows the w velocity components distribution along the centerline of cubic cavity for Re = 100 at Ri = 0.001 and 10. It was found that | w_max | decreases with the aspect ratio regardless of the Richardson number.

IV. Conclusion

In this study, we present a detailed analysis on the effect of aspect ratio Ay ranging from 0.25 to 1 in a lid driven cavity. The top moving lid of the cavity is maintained at a constant temperature, while the vertical walls are thermally insulated. The working fluid is air so that the Prandtl number equates to 0.71. The Reynolds number varied from 100 to 1000 and Richardson number ranging from 0.001 to 10. Parametric studies of the effect of the mixed convection parameter, Richardson number on the fluid flow and heat transfer have been performed. Flow and heat transfer characteristics, streamlines, isotherms and average wall Nusselt number are presented for whole range of Richardson number considered. The results indicate that for Ri = 10 The number of cells decreases with the aspect ratio and the isotherms exhibit thermal stratification for different aspect ratio and for Ri = 0.001, the current lines present a similar pattern and isotherms shows that the buoyancy effect is dominant. Also, a significant increase of the Nusselt number with the aspect ratio is observed.

V. References

[1] K.L. Wong, A.J. Baker, A 3D incompressible Navier–Stokes velocity–vorticity weak form finite element algorithm, Int. J. Numer. Methods Fluids 38 (2002) 99–123.
[2] R. Iwatsu and J.M. Hyun, Three-dimensionel driven-cavity flows with a vertical temperature gradient.
[3] A.A.Mohamed, R.Viskanta, Flow and heat transfer ina lid-driven cavity filled with a stably stratified fluid, Appl.Math. Modelling 19 (1995) 465-472.
[4] Moallemi, M. K. et Jang, K. S. (1992). Prandtl number effects on laminar mixed convection heat transfer in a lid-driven cavity. Int. J. Heat Mass Tran., Vol. 35, pp. 1881–1892.
[5] Prasad, A. K. et Koseff, J. R. (1996). Combined forced and natural convection heat transfer in a deep lid-driven cavity flow. Int. J. Heat Fluid Flow, Vol. 17, pp. 460–467.
[6]M.A.R.Sharif, Laminar mixed convection in shallow inclined driven cavities with hot moving lid on top and cooled from bottom, Applied Thermal Engineering 27 (2007) 1036-1042.
[7] Nader Ben Cheikh Effet du rapport de forme transverse sur l'écoulement tridimensionnel d'un fluide incompressible dans une cavité entraînée
[8]Fakher Oueslati, Brahim Ben BeyaAspect ratio effects on three-dimensional incompressible flow ina two-sided non-facing lid-driven parallelepiped cavity
[9] R. Peyret, T.D. Taylor, Methods for Fluid Flow, Springer-Verlag, Berlin, Germany, 1983.
[10] Y. Achdou, J.L. Guermond, Convergence analysis of a finite element projection/Lagrange Galerkin method for the incompressible Navier–Stokes equations, SIAM J. Numer. Anal. 37 (2000) 799–826.
[11] S.V. Patankar, A calculation procedure for two-dimensional elliptic situations, Numer. Heat Transfer 34 (1981) 409–425.
[12] F. Moukhalled, M. Darwish, A unified formulation of the segregated class of algorithm for fluid flow at all speeds, Numer. Heat Transfer, Part B: Fundamentals 37 (2000) 103–139.
[13] M.H. Kobayachi, J.M.C. Pereira, J.C.F. Pereira, A conservative finite-volume second-order-accurate projection method on hybrid unstructured grids, J. Comput. Phys. 150 (1999) 40–75.
[14] T. Hayase, J.A.C. Humphrey, R. Greif, A consistently formulated QUICK scheme for fast and stable convergence using finite-volume iterative calculation procedures, J. Comput. Phys. 98 (1992) 108 -118.

[15] W.H. Press, et al., second edition, Numerical Recipes in Fortran 77: The Art of Scientific Computing, vol. 1, Cambridge Press, London, UK, 1997.
[16] M. Hortmann, M. Peric, G. Scheuerer, Finite volume multigrid prediction of laminar natural convection: benchmark solutions, Int. J. Numer. Meth. Fluids 11 (1990) 189–207.
[17] M.S. Mesquita, M.J.S. de Lemos, Optimal multigrid solutions of dimensional convection–conduction problems, Appl.Math.Comput. 152 (2004) 725–742.
[18] E. Nobile, Simulation of time-dependent flow in cavities with the correction multigrid method, Part I: Mathematical formulation, Numer. Heat Transfer, Part B: Fundamentals 30 (1996) 341–350.
[19] N. Ben-Cheikh, B. Ben-Beya, T. Lili, Benchmark solution for time-dependent natural convection flows with an accelerated full-multigrid method, Num. Heat Trans. (B), 52 (2007) 131-151.